Int. J. Heat Mass Transfer. Vol. 33, No. 4, pp. 593–602, 1990
Printed in Great Britain

0017–9310/90 $3.00 + 0.00

Numerical and analytical solutions of one-dimensional freezing of dilute binary alloys with coupled heat and mass transfer

S. C. GUPTA
Department of Applied Mathematics, Indian Institute of Science, Bangalore 560012, India

(*Received* 29 *April* 1988 *and in final form* 21 *February* 1989)

Abstract—The purpose of the present study is to present simple and effective numerical and analytical solutions of one-dimensional solidification of dilute binary alloys. Although the numerical and analytical results are presented here for one-dimensional radially symmetric inward spherical solidification, the methods of solution are valid for several other one-dimensional problems. It is assumed that the heat and mass transport takes place only by diffusion and there is local thermodynamic equilibrium at the freezing front which is assumed to be planar. In the present study, solidus and liquidus curves are assumed to be linear, however, more general phase diagrams can also be accommodated. Numerical results are presented for wide ranging values of the ratios of diffusivities. The occurrence of steep concentration gradients at the freezing front does not require any special modification of the numerical scheme. Using the present analytical method, all the previously existing exact analytical solutions which pertain only to the semi-infinite region can be derived in a systematic way.

1. INTRODUCTION

DEPENDING on the assumptions made about the nature of the solid–liquid interface whether it is taken as planar or nonplanar, the literature on binary alloy solidification problems can be divided, broadly, into three classes. Class I consists of those problems in which the freezing front is taken as planar and it distinctly separates the solid region from the liquid region with no mushy zone in between. Mostly numerical solutions, and a few analytical solutions, exist for these problems. In class II problems, the solid and liquid regions are separated by a mushy zone in which solid and liquid both coexist. The fraction of the solid present in the mushy zone is approximated in some suitable way to carry out numerical computations such as in ref. [1]. As far as we know no analytical solution exists for these problems. In class III problems, the physical model is the same as in class II problems but the objective is to study the stability of the planar phase boundary, segregation, relations between the solid fraction and the temperatures in the mushy zone, etc., such as in refs. [2–4].

The present study belongs to class I problems and therefore only those previously obtained numerical and analytical solutions which use the planar phase boundary assumption will be discussed here in detail. As compared to the Stefan problems, extremely few analytical solutions of alloy solidification exist in the literature [5–7]. This is not surprising as alloy solidification is far more complicated than the Stefan problem. In the present problem the temperatures and concentrations at the freezing front are time dependent and are unknown. The freezing front is not known a priori. The concentration has an unknown time-dependent discontinuity at the freezing front. Tsubaki and Boley [5] and Rubinstein [6] have considered one-dimensional alloy solidification in a semi-infinite medium. Temperatures and concentrations at the freezing front remain fixed constants for all time. If natural convection is neglected then the solution in ref. [6] can be obtained as a particular case of the solution in ref. [5]. No systematic method of solution has been presented in these papers. In ref. [7], Boley obtained a short-time solution for a finite slab. The method of solution does not seem to be applicable to other geometries. For alloy solidification, in a spherical geometry, no analytical solution or for that matter any method of solution has been proposed earlier. The main features of the present analytical technique which is applicable to one-, two- and three-dimensional semi-infinite regions, a one-dimensional spherical cavity and one- and two-dimensional cylindrical geometrics, etc. are as follows.

The solid and liquid regions at any time are embedded in the original region occupied by the melt. This original region is then extended fictitiously and fictitious unknown initial temperatures and concentrations are assumed for the original and extended regions. These unknown initial temperatures and concentrations control the conditions at the freezing front. This central idea in the present method is independent of the boundary conditions and the geometry concerned and depends only on the availability of the source solutions.

Levin [8], Wollhöver *et al.* [9] and Derby and Brown [10] have obtained finite difference numerical solutions for a finite slab. They have neglected solute diffusion in the solid and thus considered a simplified problem. Some numerical approaches up to 1981 can

NOMENCLATURE

A_n	coefficients in equation (25)
C	dimensionless concentration of the solute in the solution
c_p	specific heat of the solid [J kg^{-1} K^{-1}]
D	diffusion coefficient [m^2 s^{-1}]
erf ( )	error function
erfc ( )	complementary error function
$f_S(v)$	dimensionless prescribed temperature in equation (2), prescribed temperature/T_A
$f_S^{(n)}$	coefficients in equation (26)
k	thermal diffusivity [m^2 s^{-1}]
K	thermal conductivity [J m^{-1} s^{-1} K^{-1}]
l	latent heat of fusion [J kg^{-1}]
m_1	slope of the liquidus line in Fig. 1
m_2	slope of the solidus line in Fig. 1
N_L	number of space grid points in the liquid
N_S	number of space grid points in the solid
p	dummy variable of integration in equations (19)–(22)
r	radial coordinate in spherical polar coordinates [m]
R	dimensionless radius of the sphere, r/R_0
R_0	radius of the sphere [m]
t	time [s]
t_0	variable having dimensions of time [s]
t_{run}	run time of the numerical scheme for complete solidification on a DEC 1090 computer [s]
T	dimensionless temperature, temperature/T_A
T_A	freezing temperature of the pure solvent [K]
V	dimensionless time for analytical solution, $2(k_S t/R_0^2)^{1/2}$
X	position of the freezing front [dimensionless], distance from the origin to the freezing front
y	dimensionless time for numerical solution, t/t_0
Δy	time step in the numerical scheme.

Greek symbols

α_1	$(k_S/k_L)^{1/2}$
α_2	$(k_S/D_S)^{1/2}$
α_3	$(k_S/D_L)^{1/2}$
β	K_L/K_S
β_1	D_L/D_S
η	$k_S t_0/R_0^2$
$\theta_i^{(1)}$, $\theta_i^{(2)}$	dimensionless initial temperatures in equations (19), (21), (23) and (24); i = L, S
λ	$l/c_p T_A$
$\phi_i^{(1)}$, $\phi_i^{(2)}$	dimensionless initial concentrations in equations (20) and (22)–(24); i = L, S.

Subscripts

L	liquid
S	solid.

be found in ref. [8]. In the semi-analytical approach adopted by Levin [8], the numerical solution is of routine type and the generalizations of the methods employed in refs. [9, 10] to suit the present problem are not known. Meyer's [11] numerical solution pertains to a two-phase coupled problem but is complicated, at least, as compared to the present work. We shall discuss Meyer's solution subsequently after the present numerical scheme has been described. Crowley and Ockendon [12] and Wilson *et al.* [13] have used an enthalpy method for numerical solutions of a finite slab. Both these works suffer from the disadvantage that when the thermal and mass diffusivities are different in the solid and liquid phases, respectively, some modified values are assigned to these parameter values. The validity of these modified values does not follow from any physical law but they are accepted since the numerical values compare well with Rubinstein's solution [6] which is a special type of solution in which the melting temperature is independent of time. Only explicit finite difference schemes have been used in refs. [12, 13] which are generally unsuitable for longer times. In the present study, the idea of moving grid points [14] has been suitably exploited to suit the coupled problem. After overcoming the difficulties encountered, an accurate procedure has been indicated which is readily applicable at least to class I problems.

In all the works [8–13] reported earlier, the solid–liquid interface has been assumed to be planar and the effects of advection in the melt have been neglected which is also the case in the present study. In rapid solidification of alloys, the physical model assuming a planar phase boundary adequately represents the real situation [15]. Recently Trivedi [16] has given a criteria according to which the existence of a planar phase boundary could be predicted. This is just to emphasize that, depending on the parameter values, there could be situations in which the mushy region may not occur or its effect may not be significant. We shall see later that in Figs. 2 and 3 of this paper, no mushy region occurs. However, it cannot be denied

that in many situations the planar phase boundary model is inadequate and also advective terms in the melt region cannot be neglected.

The main purpose of the present study is to present simple and effective numerical and analytical solutions of class I problems which are till now missing in the literature. Since the present numerical scheme is valid for diffusion in both the phases and the parameters can have wide ranging values, it is hoped that this study will help in a better understanding of the alloy solidification process.

2. PROBLEM FORMULATION

Consider a binary alloy of two components A and B which is in the liquid state at time $t = 0$ and occupies the spherical region $0 \leqslant R \leqslant 1$ (one-dimensional radially symmetric problem). Component B forms a dilute solution in component A. The alloy is cooled at the surface $R = 1$ and the temperature is prescribed there. If the prescribed surface temperature satisfies certain conditions which are discussed below in equations (17) and (18) then the solidification will start at the boundary and with time, the solid–liquid interface which is assumed to be sharp, will progress towards the interior till the whole of the alloy gets solidified. It is assumed that there is local thermodynamic equilibrium at the freezing front and solidus and liquidus curves are linear as indicated in Fig. 1. The problem under consideration is to find the temperature and concentration profiles in the solid and liquid regions and the freezing front satisfying the following dimensionless differential equations, initial, boundary and interface conditions.

Solid region

$$2\frac{\partial T_S}{\partial V} = \frac{V}{R}\frac{\partial^2}{\partial R^2}(RT_S), \quad X(V) \leqslant R \leqslant 1, \; V > 0 \tag{1}$$

$$T_S|_{R=1} = f_S(V), \quad V \geqslant 0 \tag{2}$$

$$2\alpha_2^2\frac{\partial C_S}{\partial V} = \frac{V}{R}\frac{\partial^2}{\partial R^2}(RC_S), \quad X(V) \leqslant R \leqslant 1, \; V > 0 \tag{3}$$

$$\left.\frac{\partial C_S}{\partial R}\right|_{R=1} = 0, \quad V \geqslant 0. \tag{4}$$

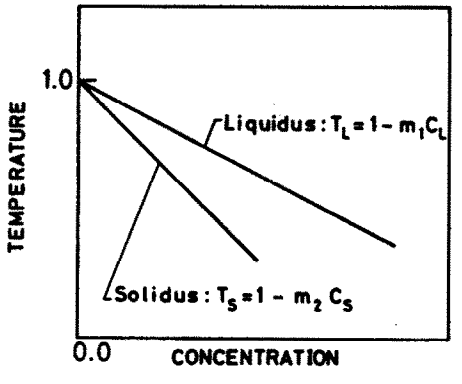

FIG. 1. Linearized phase diagram for a dilute binary alloy.

Liquid region

$$2\alpha_1^2\frac{\partial T_L}{\partial V} = \frac{V}{R}\frac{\partial^2(RT_L)}{\partial R^2}, \quad 0 \leqslant R < X(V), \; V > 0 \tag{5}$$

$$T_L|_{V=0} = \theta_L^{(1)}(R), \quad 0 \leqslant R \leqslant 1 \tag{6}$$

$$\left.\frac{\partial T_L}{\partial R}\right|_{R=0} = 0 \tag{7}$$

$$2\alpha_3^2\frac{\partial C_L}{\partial V} = \frac{V}{R}\frac{\partial^2}{\partial R^2}(RG_L), \quad 0 \leqslant R < X(V), \; V > 0 \tag{8}$$

$$C_L|_{V=0} = \phi_L^{(1)}(R), \quad 0 \leqslant R \leqslant 1 \tag{9}$$

$$\left.\frac{\partial C_L}{\partial R}\right|_{R=0} = 0. \tag{10}$$

Solid–liquid interface conditions

$$\left.\frac{\partial T_S}{\partial R}\right|_{R=X} - \beta\left.\frac{\partial T_L}{\partial R}\right|_{R=X} = \frac{2\lambda}{V}\frac{dX}{dV} \tag{11}$$

$$\left.\frac{\partial C_S}{\partial R}\right|_{R=X} - \beta_1\left.\frac{\partial C_L}{\partial R}\right|_{R=X} = \frac{2\alpha_2^2(1-m_1/m_2)}{V}C_L|_{R=X}\frac{dX}{dV} \tag{12}$$

$$T_L|_{R=X} = 1 - m_1 C_L|_{R=X} \tag{13}$$

$$T_S|_{R=X} = 1 - m_2 C_S|_{R=X} \tag{14}$$

$$m_2 C_S|_{R=X} = m_1 C_L|_{R=X} \tag{15}$$

$$X(0) = 1. \tag{16}$$

Equations (1) and (5) are the heat conduction equations and equations (3) and (8) the mass diffusion equations. Equations (2) and (4) are the prescribed boundary conditions at $R = 1$ which could be time dependent and equations (6) and (9) are the initial conditions which could be space dependent. Equations (11) and (12) are the heat balance and mass balance conditions, respectively, at the interface. The liquidus line is given by equation (13) and the solidus line by equation (14). Temperature is continuous across the interface. $m_1 \gtrless 0$ depending on whether $m_1/m_2 \lesssim 1$. All physical parameters are taken as constants but they could be different for different phases. Both the phases have the same density and so there is no natural convection in the melt. For the commencement of the solidification at $R = 1$ at time $V = 0$, we must have

$$\theta_L^{(1)}(R) \leqslant 1 - m_1\phi_L^{(1)}(1), \quad 0 \leqslant R \leqslant 1 \tag{17}$$

$$f_S(V) \leqslant 1 - m_1\phi_L^{(1)}(1), \quad V \geqslant 0. \tag{18}$$

Without any loss of generality it can be assumed that the solidification commences at $R = 1$ at time $V = 0$. Because, if the solidification starts at $V = V_0$, $V_0 > 0$, the concentration of the liquid remains unchanged for $0 \leqslant V \leqslant V_0$ and $\theta_L^{(1)}(R)$ can be regarded as the temperature of the liquid at $V = V_0$.

3. METHOD OF SOLUTION AND ANALYTICAL RESULTS

The solutions of equations (1), (3), (5) and (8) can be written as follows:

$$T_S = \frac{1}{\sqrt{\pi R V}}\left[\int_0^1 p\, e^{-(R-p)^2/V^2}\,\theta_S^{(1)}(p)\,dp + \int_1^\infty p\, e^{-(R-p)^2/V^2}\,\theta_S^{(2)}(p)\,dp\right], \quad 0 \leqslant R < \infty,\ V > 0 \tag{19}$$

$$C_S = \frac{\alpha_2}{\sqrt{\pi R V}}\left[\int_0^1 p\, e^{-\alpha_2^2(R-p)^2/V^2}\,\phi_S^{(1)}(p)\,dp + \int_1^\infty p\, e^{-\alpha_2^2(R-p)^2/V^2}\,\phi_S^{(2)}(p)\,dp\right], \quad 0 \leqslant R < \infty,\ V > 0 \tag{20}$$

$$T_L = \frac{\alpha_1}{\sqrt{\pi R V}}\left[\int_0^1 p\,\{e^{-\alpha_1^2(R-p)^2/V^2} - e^{-\alpha_1^2(R+p)^2/V^2}\}\cdot\theta_L^{(1)}(p)\,dp + \int_1^\infty p\,\{e^{-\alpha_1^2(R-p)^2/V^2} - e^{-\alpha_1^2(R+p)^2/V^2}\}\cdot\theta_L^{(2)}(p)\,dp\right], \quad 0 \leqslant R < \infty,\ V > 0 \tag{21}$$

$$C_L = \frac{\alpha_3}{\sqrt{\pi R V}}\left[\int_0^1 p\,\{e^{-\alpha_3^2(R-p)^2/V^2} - e^{\alpha_3^2(R+p)^2/V^2}\}\cdot\phi_L^{(1)}(p)\,dp + \int_1^\infty p\,\{e^{-\alpha_3^2(R-p)^2/V^2} - e^{-\alpha_3^2(R+p)^2/V^2}\}\cdot\phi_L^{(2)}(p)\,dp\right], \quad 0 \leqslant R < \infty,\ V > 0. \tag{22}$$

It can be checked that T_L in equation (21) satisfies conditions (6) and (7) and C_L in equation (22) satisfies conditions (9) and (10). The initial temperatures $\theta_S^{(1)}$, $\theta_S^{(2)}$ and $\theta_L^{(2)}$ and initial concentrations $\phi_S^{(1)}$, $\phi_S^{(2)}$ and $\phi_L^{(2)}$ are fictitious and are unknown. They play an important role in satisfying the boundary conditions at the freezing front. Mathematically there are seven unknowns and seven conditions to be satisfied. The following series expansions for the known and unknown functions will be assumed:

$$(\theta_i^{(1)}, \phi_i^{(1)}) = \sum_{n=0}^{\infty} (R-1)^n \left.\frac{\partial^n(\theta_i^{(1)}, \phi_i^{(1)})}{\lfloor n\, \partial R^n}\right|_{R=1}, \quad 0 \leqslant R \leqslant 1;\ i = L, S \tag{23}$$

$$(\theta_i^{(2)}, \phi_i^{(2)}) = \sum_{n=0}^{\infty} (R-1)^n \left.\frac{\partial^n(\theta_i^{(2)}, \phi_i^{(2)})}{\lfloor n\, \partial R^n}\right|_{R=1}, \quad 1 < R < \infty;\ i = L, S \tag{24}$$

$$X(V) = 1 + \sum_{n=1}^{\infty} A_n V^n, \quad V \geqslant 0 \tag{25}$$

$$f_S(V) = \sum_{n=0}^{\infty} f_S^{(n)} V^{(n)}, \quad V \geqslant 0. \tag{26}$$

The problem now is to determine the unknown coefficients occurring in equations (23)–(25). The method of determining unknowns is similar to the one described in detail in earlier works [17, 18] in which Stefan problems have been studied. Just for completeness sake we mention here that the solutions given in equations (19)–(22) are substituted in equations (2), (4), (10)–(13) and (15) and the nth derivatives of these equations for $n = 0, 1, 2, \ldots$, with respect to V are obtained. The unknown coefficients can be determined in a systematic way by taking the limits $V \to 0+$ of these equations. The details of the algebra are not given here. The coefficient A_1 in the moving boundary and some related quantities are given below. In the numerical work, the coefficient A_2 was also included but is not given here to save space

$$2\sqrt{\pi\lambda}A_1 = 2\, e^{-A_1^2}\{f_S^{(0)} - \theta_S^{(1)}(1)\} - \alpha_1\beta\, e^{-A_1^2\alpha_1^2}\{\theta_L^{(2)}(1) - \theta_L^{(1)}(1)\} \tag{27}$$

$$\operatorname{erf}(A_1)\theta_S^1(1) = \{1 + \operatorname{erf}(A_1)\}f_S^{(0)} - 1 + m_2\phi_S^{(1)} \tag{28}$$

$$\theta_S^{(2)}(1) = 2f_S^{(0)} - \theta_S^{(1)}(1) \tag{29}$$

$$\{1 + \operatorname{erf}(A_1\alpha_1)\}\theta_L^{(2)}(1) = 2 - 2m_2\phi_S^{(1)}(1) \tag{30}$$

$$2m_2\phi_S^{(1)}(1) = m_1[\operatorname{erfc}(A_1\alpha_3)\phi_L^{(1)}(1) + \{1 + \operatorname{erf}(A_1\alpha_3)\}\phi_L^{(2)}(1)] \tag{31}$$

$$\phi_S^{(2)}(1) = \phi_S^{(1)}(1) \tag{32}$$

$$[\sqrt{\pi}\alpha_2^2 A_1(1 - m_1/m_2)\{1 + \operatorname{erf}(A_1\alpha_3)\} + \alpha_3\beta_1\, e^{-A_1^2\alpha_3^2}]\phi_L^{(2)}(1) = [\alpha_3\beta_1\, e^{-A_1^2\alpha_3^2} - \sqrt{\pi}\alpha_2^2(1 - m_1/m_2)A_1 \operatorname{erfc}(A_1\alpha_3)]\phi_L^{(1)}(1). \tag{33}$$

The numerical values of A_1 and A_2 from their analytical expressions can be easily calculated. In principle, the coefficients A_3, A_4, etc. in the moving boundary can also be calculated but the algebra becomes extremely lengthy. Along with the unknowns of the moving boundary, the unknowns in the temperature and concentration solutions are also determined. The temperature $T_L(R, V)$ in the liquid region which is valid for small V and small $|R-1|$ is given as

$$T_L(R, V) = \tfrac{1}{2}\operatorname{erfc}\{\alpha_1(R-1)/V\} \times \left\{\theta_L^{(1)}(1) + (R-1)\left.\frac{\partial\theta_L^{(1)}}{\partial R}\right|_{R=1}\right\} - \frac{V}{(2\sqrt{\pi}\alpha_1^2 R)} \times \left\{\theta_L^1(1) + (2R-1)\left.\frac{\partial\theta_L^{(1)}}{\partial R}\right|_{R=1}\right\} \times \exp\{-\alpha_1^2(R-1)^2/V^2\} + \tfrac{1}{2}[2 - \operatorname{erfc}\{\alpha_1(R-1)/V\}]\left\{\theta_L^{(2)}(1) + (R-1)\right.$$

$$\times \left.\frac{\partial \theta_L^{(2)}}{\partial R}\right|_{R=1} \Bigg\} + \frac{V}{(2\sqrt{\pi R \alpha_1})} \Bigg\{ \theta_L^{(2)}(1) + (2R-1) \times \left.\frac{\partial \theta_L^{(2)}}{\partial R}\right|_{R=1} \Bigg\} \exp\{-\alpha_1^2 (R-1)^2 / V^2\}$$

+ terms of the type $(R-1)^m V^n$,

$$\text{where} \quad m+n \geqslant 2,\ V>0,\ R>0. \quad (34)$$

The derivation of the above solution is similar to the solutions discussed in detail in refs. [17, 18] in which the justification of the method of solution, justification of the series expansions for known and unknown functions, the time for which the short-time solution is valid, etc. have also been discussed in the context of Stefan problems. To determine $T_S(R, V)$, put $\alpha_1 = 1$ and replace the subscript L by subscript S everywhere in equation (34). $C_S(R, V)$ and $C_L(R, V)$ can be determined by putting $\alpha_1 = \alpha_2$ and $\alpha_1 = \alpha_3$, respectively, in equation (34) and replacing θ by ϕ everywhere.

4. FURTHER APPLICATIONS OF THE ABOVE METHOD

By choosing an appropriate source solution and using the above method of analytical solution, the solution of several coupled heat and mass transfer problems pertaining to a semi-infinite medium, cylindrical geometries and an infinite medium with a spherical hole, etc. can be obtained. The boundary conditions prescribed at the fixed boundaries of the regions considered could be of the first, second or third kind. It may be pointed out here that once an appropriate source solution is chosen for the region under consideration and temperature and concentration solutions are written down in terms of the source solution, the method of solution remains the same as described above and only the details of the algebra change. Although the details of the algebra have been avoided here to save space, it may be mentioned that the present solution is obtained in a systematic and straightforward manner. The solution so obtained is in general a short-time solution. However, in some cases, such as the problem considered by Tsubaki and Boley [5], an exact analytical solution can be obtained by the present method which agrees with the solution given in ref. [6]. The additional advantage in the present method is that the solution is obtained in a systematic way and does not depend on the fortuitous choice of functions.

5. NUMERICAL SOLUTION AND DISCUSSION

The method of numerical solution will be discussed here in some detail so as to make it useful to the reader. The emphasis is more on showing the feasibility of the numerical scheme for a wide range of parameter values and also to indicate the ease with which the numerical scheme can handle sharp concentration gradients near the phase boundary. Because of these priorities, no extensive study of any alloy has been done in particular.

The main feature of the Murray and Landis finite difference numerical scheme [14] is that the space grid points move with the freezing front position. An efficient execution of this numerical scheme for a one-dimensional Stefan problem has been recently proposed [18]. The present numerical work concerning the alloy solidification is a suitable adaptation of the previous work. The major hurdles one comes across in the coupled problem are the determination of the temperature or the concentration at the freezing front which is not known a priori, and, the handling of the sharp concentration gradients at the freezing front. A very large number of numerical experiments were carried out to arrive at an appropriate execution of the numerical scheme which in essence is as follows.

The dimensionless times used for analytical and numerical works are V and y, respectively. After assigning appropriate velocities to the space nodal points, the finite difference discretization of the heat equations (1) and (5) and mass diffusion equations (3) and (8) can be carried out using the implicit scheme. For example equation (8) can be discretized as

$$\frac{C_L^{iJ+1} - C_L^{iJ}}{\Delta y} = \frac{\eta}{\alpha_3^2 \Delta R_L^2} \{C_L^{i+1,J+1} - 2C_L^{iJ+1} + C_L^{i-1,J+1}\} + \frac{1}{2\Delta R_L}(C_L^{i+1,J+1} - C_L^{i-1,J+1}) \times \left\{\frac{(X^{J+1} - X^J)(N_L - 1 - i)R_L}{\Delta y X^{J+1}} + \frac{2\eta}{\alpha_3^2 i \Delta R_L}\right\},$$

$$i = 1, 2, \ldots, N_L;\ J = 0, 1, 2, 3, \ldots \quad (35)$$

Superscript i indicates that the quantity is evaluated at the ith nodal point and superscript J indicates that the quantity is evaluated at time $J\Delta y$; ΔR_L is the uniform distance between any two space nodal points in the liquid region. The nodal point $i = 0$ corresponds to the point at the moving interface. Suppose that the freezing front, temperatures and concentrations are known at time $J\Delta y$. Equation (12) can then be used to determine a first approximation of X^{J+1} in which the concentration derivatives are calculated at time $J\Delta y$ using three point formulas. Equation (11) is then used to obtain a first approximation of T_S at X^{J+1} and at time $(J+1)\Delta y$. In doing so, some of the quantities are not known at $y = (J+1)\Delta y$; therefore their values at time $J\Delta y$ are substituted instead. Temperatures and concentrations at all the space nodal points and at time $y = (J+1)\Delta y$ can now be calculated from the discretized equations (1), (5), (3) and (8).

A second approximation of X^{J+1} is obtained from equation (12) in which the concentration derivatives are now calculated at time $(J+1)\Delta y$. A second approximation of T_S at X^{J+1} and at time $(J+1)\Delta y$ is then obtained from equation (11). X^{J+1} was iterated till the absolute difference between successive iter-

ations became less than 10^{-6}. At subsequent times, the various quantities were again calculated in the manner indicated above. At time $y = \Delta y$, the analytical values of freezing front, temperatures and concentrations in the solidified thickness were used in the numerical scheme. The analytical solution was not used afterwards at any other time. It may be remarked here that based on the above procedure, several ways of determining moving boundary, temperatures, etc. can be thought of and many of them were tried. The procedure listed above was found to be the most stable and accurate.

The determination of the freezing front and freezing temperature in Meyer's work (refer to equations (15) and (16) in ref. [11]) does not seem to be as simple and straightforward as in the present numerical scheme.

A large number of numerical experiments were carried out and it can be said that successive iterations do converge, in the sense that the difference between two successive iterations becomes less than 10^{-6} for wide ranges of parameter values. Do the iterations converge to the correct value? To verify this, several analytical and numerical checks are available. In Table 1, the numerical solution has been compared with the analytical solution for two sets of parameter values. The analytical solution is a short-time solution and is valid for small values of V and $|R-1|$ (refer to refs. [17, 18] also) and therefore, temperatures and concentrations in the liquid cannot be compared with the numerical solution at all the space grid points. It may be noted that in Table 1 for $V = 0.15$, the numerical scheme has run for about 20 time steps with $\Delta y = 0.001$ and the good agreement between the analytical and numerical solutions is in order. The integral mass balance check provides a useful numerical check. A second numerical check is provided by the stability of the numerical results when the time step is halved and the number of space grid points is doubled. Later, these numerical checks have been discussed further in the context of the figures drawn.

In accordance with the physical and mathematical model considered in equations (1)–(14), the solid–liquid interface at any time divides the region $0 \leqslant R \leqslant 1$, into two distinct regions, namely, solid and liquid regions. Our mathematical and numerical models do not account for the existence of the mushy region. The temperatures of the points lying in the region $X(V) \leqslant R \leqslant 1$ should be less than or equal to $T_S|_{R=X}$. These points will constitute a solid region. The temperatures of the points lying in the region $0 \leqslant R \leqslant X(V)$ should be greater than or equal to $T_S|_{R=X}$. These points will constitute a liquid region. If the numerical values of the temperatures do not satisfy the above criterion then they are inconsistent with the physical model considered in class I problems and such values will be regarded as inaccurate. In none of the numerical experiments conducted in this study, were inconsistent values obtained.

In Fig. 1, the solidus and liquidus lines are defined by equations (13) and (14). The phase diagram in Fig. 1, is interpreted as follows.

If the point (C, T) lies above the liquidus line then it is in a stable liquid phase, while if the point (C, T) lies below the solidus line then it is in a stable solid phase. If the point (C, T) lies in the region between the liquidus and solidus lines, it is regarded as a point in the mushy region. Wilson *et al.* [19] have interpreted the numerical results of Rubinstein's solution [6] pertaining to a class I problem according to the above criterion and pointed out the existence of an artificial mushy region just in front of the interface. The term artificial is justified here as in class I problems, only solid and liquid regions exist. In Figs. 2 and 3 of this paper, no artificial mushy region occurs but in Figs. 4–8 it does.

In Figs. 2–8, temperatures, concentrations and

Table 1. Comparison of the numerical solution with the short-time analytical solution for two sets of parameter values. First set of parameter values: $\alpha_1 = 3, \alpha_2 = 1, \alpha_3 = 3, \lambda = 1.5, \beta = 2.0, m_1 = 0.4, m_2 = 0.6, \theta_L^{(1)}(R) = 1.1, \phi_L^{(1)}(R) = 0.1, f_S(V) = 0.8$

V	Temperatures in the solid at the points† R_1	R_2	R_3	Concentrations in the solid at the points R_1	R_2	R_3	Freezing front $X(V)$
0.077	0.9545‡	0.8777	0.8010	0.0763	0.0763	0.0762	0.9925
	0.9546	0.8772	0.8000	0.0756	0.0756	0.0756	0.9939
0.15	0.9554	0.8797	0.8047	0.0762	0.0762	0.0761	0.9853
	0.9541	0.8767	0.8000	0.0763	0.0764	0.0764	0.9861

Second set of parameter values: $\alpha_1 = 3, \alpha_2 = 50, \alpha_3 = 20, \lambda = 1.5, \beta = 2.0, m_1 = 0.4, m_2 = 0.6, \theta_L^{(1)}(R) = 1.1, \phi_L^{(1)}(R) = 0.1, f_S(V) = 0.8$

0.077	0.9422	0.8715	0.8009	0.0967	0.0956	0.0944	0.9933
	0.9430	0.8714	0.8000	0.0951	0.0948	0.0947	0.9942
0.15	0.9415	0.8726	0.8042	0.0993	0.0969	0.0944	0.9869
	0.9406	0.8700	0.8000	0.0990	0.0976	0.0948	0.9871

† $R_{i+1} = X(V) + i(1 - X(V))/2, i = 0, 1, 2.$

‡ Upper and lower values are analytical and numerical values, respectively.

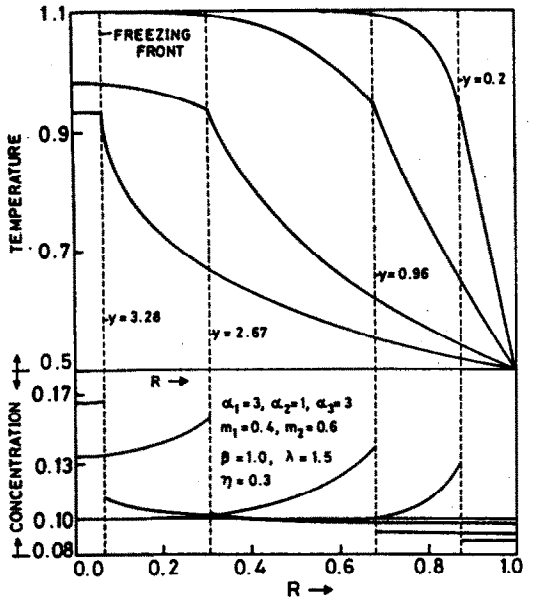

FIG. 2. Temperatures, concentrations and freezing front. t_{run} = about 6 min. $\theta_L^{(1)}(R) = 1.1$, $\phi_L^{(1)}(R) = 0.1$, $f_S(V) = 0.5$, $\Delta y = 0.01$, $N_S = 101$, $N_L = 401$.

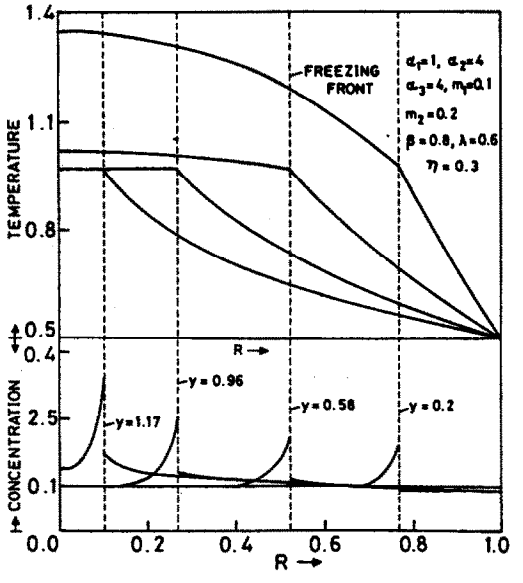

FIG. 4. Temperatures, concentrations and freezing front. t_{run} = about 7 min. $\theta_L^{(1)}(R) = 1.4$, $\phi_L^{(1)}(R) = 0.1$, $f_S(V) = 0.5$, $\Delta y = 0.01$, $N_S = 101$, $N_L = 401$.

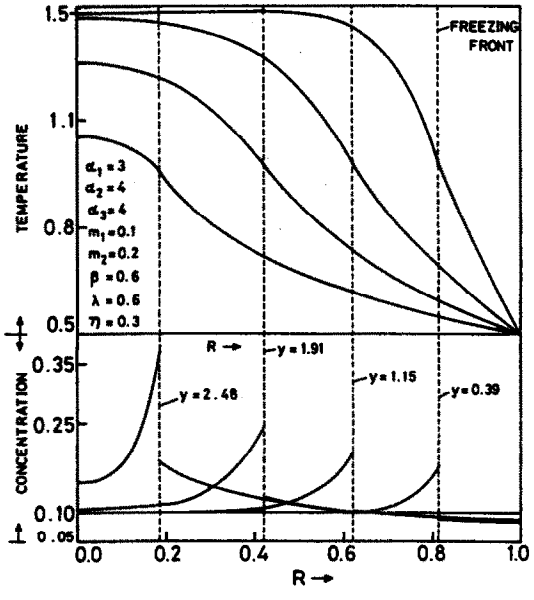

FIG. 3. Temperatures, concentrations and freezing front. t_{run} = about 6 min. $\theta_L^{(1)}(R) = 1.4$, $\phi_L^{(1)}(R) = 0.1$, $f_S(V) = 0.5$, $N_S = 101$, $N_L = 401$, $\Delta y = 0.01$.

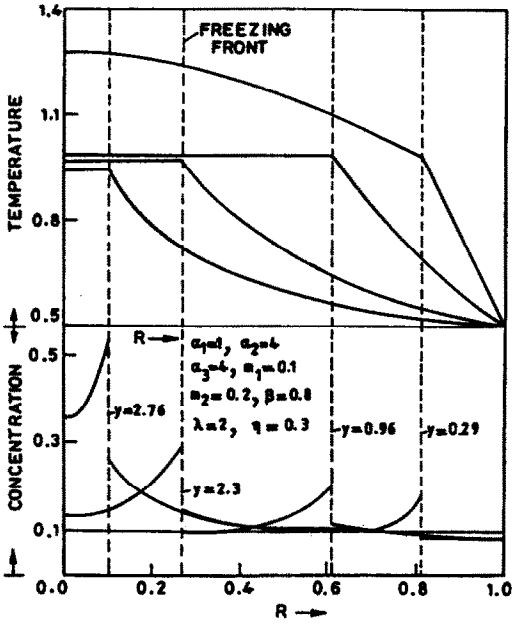

FIG. 5. Temperatures, concentrations and freezing front. t_{run} = about 6 min. $\theta_L^{(1)}(R) = 1.4$, $\phi_L^{(1)}(R) = 0.1$, $f_S(V) = 0.5$, $\Delta y = 0.01$, $N_S = 101$, $N_L = 401$.

freezing front are shown for different sets of parameter values. The boundary temperatures, initial temperatures and initial concentrations have been taken as constants. Since there are in general sharp concentration gradients around the freezing front, the number of space grid points N_L and N_S have to be larger as compared to the Stefan problem of the same geometry. In the captions to the figures, the values of N_S, N_L, the computer run time, etc. are also given.

The numerical work involves a large number of parameters. It seems difficult to associate a particular effect in the graphs with a specific parameter with certainty, more so, when the numerical work was done mostly to show the feasibility of the numerical scheme, but still some observations can be made. In Fig. 2, the ratios k_S/D_S and k_L/D_L are both equal to one. Numerical results were also obtained for $\beta = 2.0$ and other parameters remaining the same as in Fig. 2

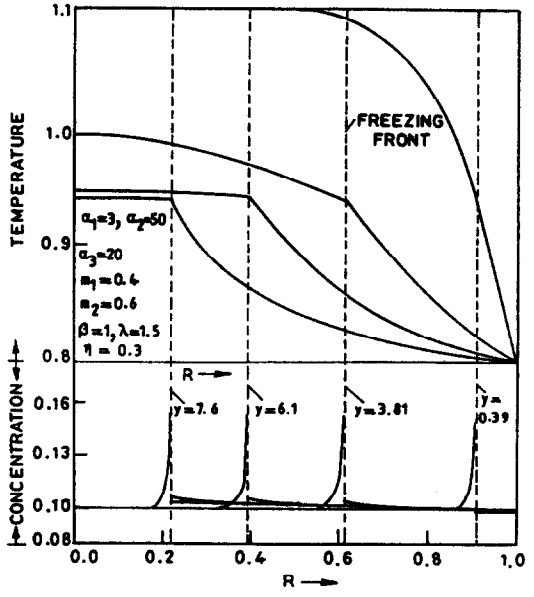

FIG. 6. Temperatures, concentrations and freezing front. t_{run} = about 6.5 min. $\theta_L^{(1)}(R) = 1.1$, $\phi_L^{(1)}(R) = 0.1$, $f_S(V) = 0.8$, $\Delta y = 0.01$, $N_S = 161$, $N_L = 801$.

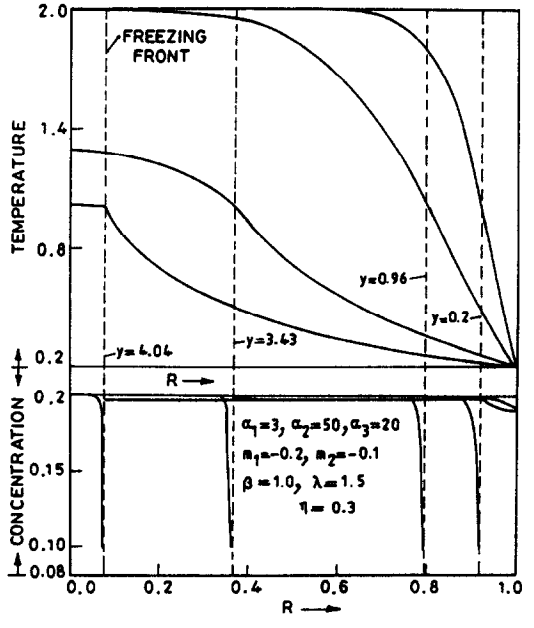

FIG. 7. Temperatures, concentrations and freezing front. t_{run} = about 6.25 min. $\theta_L^{(1)}(R) = 2.0$, $\phi_L^{(1)}(R) = 0.2$, $f_S(V) = 0.2$. $\Delta y = 0.01$, $N_S = 161$, $N_L = 801$.

but are not reported here to save space. In both cases, no artificial mushy region occurs. In the latter case, the total solidification time increases by about 25% but if one compares the temperatures and concentrations with those in Fig. 2 at the same freezing front position then the maximum difference found is about 2–3% which occurs at points far away from the freezing front. In Fig. 3, the ratio $k_L/D_l = 1.8$. No artificial mushy zone occurs. In Figs. 2–5, for larger

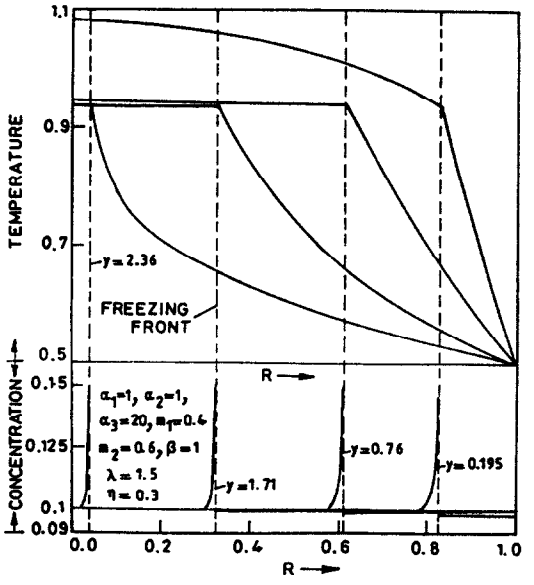

FIG. 8. Temperatures, concentrations and freezing front. t_{run} = about 8.25 min. $\theta_L^{(1)}(R) = 1.1$, $\phi_L^{(1)}(R) = 0.1$, $f_S(V) = 0.5$, $\Delta y = 0.005$, $N_S = 161$, $N_L = 801$.

times, the concentration has significantly changed at all points of the region $0 \leqslant R \leqslant X$ but in Figs. 6–8, even for larger times, the concentration changes are confined only to a small neighbourhood of the freezing front. This effect could be due to larger values of α_3 in Figs. 6–8 than in Figs. 2–5.

In Figs. 2–5, all the parametric values are neither too high nor too low. The numerical scheme in all such cases was found to run fairly smoothly, in the sense that successive iterations converge fast, the integral mass balance check can be satisfied almost exactly, the variations in temperatures, concentrations and freezing front values can be made insignificant for small changes in the time step and the number of space grid points by appropriately choosing Δy, N_S and N_L.

In Figs. 4–8, for larger times, the temperature curves in the region $0 \leqslant R < X$ have become horizontal lines and this could be attributed to the large values of the ratio k_L/D_L. However, initial and boundary temperatures also play a role in this. The high thermal diffusivity in the liquid seems to be responsible in reducing total solidification times in Figs. 4 and 8. In Fig. 6, the large solidification time is due to the high value of the prescribed boundary temperature. Numerical results were also obtained for a prescribed boundary temperature equal to 0.5 in Fig. 6 and the total solidification time is reduced to less than half of that in Fig. 6. In Fig. 7, m_1 and m_2 have negative values. The maximum error in the integral mass balance check was found to be less than 0.3% in Figs. 2–5 and the same error in Figs. 6–8 is less than 1%.

Several trial runs were carried out for the cases in which $m_1 = 4$, $m_2 = 20$, $\alpha_1 = 1$, $\alpha_2 = 20$, $\alpha_3 = 1$ (the case of low solute diffusion in the solid) remained

fixed and other parameters were varied. The numerical scheme works alright but it takes a very long time. In about 6 min computer run time, the maximum solidified thickness obtained was about 0.2 indicating that for some limiting cases convergence could be slow.

Apart from some specific comments made earlier about the numerical work, the following general comments can be made.

(1) A 1 or 2% error in the integral mass balance check was not found to be a serious problem provided the error changes only marginally with time say, from 2% it becomes about 2.5% during total solidification. Whenever this error remained stable, it was possible to make it insignificant by a suitable choice of Δy, N_L and N_S.

(2) The freezing front and temperature values were found to be fairly stable with respect to changes in Δy, N_L and N_S but concentration values especially near the boundary $R = 1$ varied in some cases by 1–3%. If one is prepared to accept an error of 1–2% in the temperatures and freezing front values and about 5–15% in concentration values, then the computer run time can be considerably reduced by using a smaller number of grid points, e.g. $N_S = 41$ and $N_L = 121$.

(3) It is often not possible to relax the convergence criterion of successive iterations, i.e. go to the next time step if the absolute difference between successive iterations becomes less than 10^{-5} or 10^{-4}, etc. as in some cases the results became absurd after some time steps.

Some comparison of general features of the numerical results obtained here can be carried out with experimental data. However, checking of numerical values with experimental values is generally difficult unless the experiments are performed in accordance with the mathematical model and experimental values are available. It is well known that for short time the solid–liquid interface in a spherical problem has the same pattern of growth as in the slab problem. In Fig. 5 of ref. [4] some experimental results are given for unidirectional solidification in a slab. The solid–liquid interface has been found to vary as the square root of time. Also in Figs. 2–8 we found that for a solidified thickness up to 0.2 approximately, the solid–liquid interface varies as the square root of time. The results for Fig. 5 in the present work are given in which maximum artificial mushy region occurs. For $V = 0.34$, 0.48, 0.59, the solidified thickness is equal to 0.108, 0.153, 0.190, respectively.

Acknowledgement—The author would like to thank Professor A. K. Lahiri, Department of Metallurgy, and Professor P. L. Sachdev, Department of Applied Mathematics, Indian Institute of Science, for some useful suggestions during the preparation of this manuscript.

REFERENCES

1. W. D. Bennon and F. P. Incropera, A continuum model for momentum, heat and species transport in binary solid–liquid phase change systems—II. Application to solidification in a rectangular cavity, *Int. J. Heat Mass Transfer* **30**, 2171–2187 (1987).
2. W. W. Mullins and R. K. Sekerka, Stability of a planar interface during solidification of a dilute binary alloy, *J. Appl. Phys.* **35**, 444–451 (1964).
3. K. Wollhöver, M. W. Scheiwe, U. Hartmann and Ch. Körber, On morphological stability of planar phase boundaries during unidirectional transient solidification of binary aqueous solutions, *Int. J. Heat Mass Transfer* **28**, 897–902 (1985).
4. T. Fujimura and J. K. Brimacombe, Mathematical analysis of solidification behavior of multicomponent alloys, *Trans. Iron Steel Inst. Japan* **26**, 532–539 (1986).
5. T. Tsubaki and B. A. Boley, One-dimensional solidification of binary mixtures, *Mech. Res. Commun.* **4**, 115–122 (1977).
6. L. I. Rubinstein, Crystallization of a binary alloy. In *The Stefan Problem*, Section 3 of Chap. 2, pp. 52–60. English translation published by the American Mathematical Society (1967).
7. B. A. Boley, Time-dependent solidification of binary mixtures, *Int. J. Heat Mass Transfer* **21**, 824–826 (1978).
8. R. L. Levin, The freezing of finite domain aqueous solutions: solute redistribution, *Int. J. Heat Mass Transfer* **24**, 1443–1455 (1981).
9. K. Wollhöver, Ch. Körber, M. W. Scheiwe and U. Hartmann, Unidirectional freezing of binary aqueous solutions: an analysis of transient diffusion of heat and mass, *Int. J. Heat Mass Transfer* **28**, 761–769 (1985).
10. J. J. Derby and R. A. Brown, A fully implicit method for simulation of the one-dimensional solidification of a binary alloy, *Chem. Engng Sci.* **41**, 37–46 (1986).
11. G. H. Meyer, A numerical method for the solidification of a binary alloy, *Int. J. Heat Mass Transfer* **24**, 778–781 (1981).
12. A. B. Crowley and J. R. Ockendon, On the numerical solution of an alloy solidification problem, *Int. J. Heat Mass Transfer* **22**, 941–947 (1979).
13. D. G. Wilson, A. D. Solomon and V. Alexiades, A model of binary alloy solidification, *Int. J. Numer. Meth. Engng* **20**, 1067–1084 (1984).
14. W. D. Murray and F. Landis, Numerical and machine solutions of transient heat conduction problems involving melting or freezing. Part I. Method of analysis and sample solutions, *ASME J. Heat Transfer* **81**, 106–112 (1959).
15. M. C. Flemings, *Solidification Processing*, p. 59. McGraw-Hill, New York (1974).
16. R. Trivedi, Theory of dendritic growth during the unidirectional solidification of binary alloys, *J. Crystal Growth* **49**, 218–232 (1980).
17. S. C. Gupta, Temperature and moving boundary in two-phase freezing due to an axisymmetric cold spot, *Q. Appl. Math.* **45**, 205–214 (1987).
18. S. C. Gupta, Analytical and numerical solutions of radially symmetric inward solidification problems in spherical geometry, *Int. J. Heat Mass Transfer* **30**, 2611–2616 (1987).
19. D. G. Wilson, A. D. Solomon and V. Alexiades, A shortcoming of the explicit solution for the binary alloy solidification problem, *Lett. Heat Mass Transfer* **9**, 421–428 (1982).

SOLUTIONS NUMERIQUES ET ANALYTIQUES DU GEL MONODIMENSIONNEL D'ALLIAGES BINAIRES DILUES, AVEC COUPLAGE DES TRANSFERTS DE CHALEUR ET DE MASSE

Résumé—Cette étude veut présenter des solutions numériques simples, efficaces et des solutions analytiques de la solidification d'alliages binaires dilués. Bien que les résultats numériques et analytiques sont présentés ici pour la solidification externe à symétrie sphérique, les méthodes de résolution sont valables pour plusieurs autres problèmes monodimensionnels. On suppose que le transfert de chaleur et de masse n'a lieu que par diffusion et qu'il y a équilibre thermodynamique local sur le front de solidification qui est supposé planaire. Dans cette étude, les courbes de solidus et liquidus sont supposées linéaires, bien que des diagrammes de phase plus généraux puissent être considérés. Des résultats numériques sont présentés pour des larges domaines de rapport de diffusivités. L'existence de gradients brusques de concentration au front ne nécessite aucune modification spéciale du schéma numérique. En utilisant la présente méthode analytique, toutes les solutions analytiques antérieures pour une région semi-infinie, peuvent être traitées d'une façon systématique.

NUMERISCHE UND ANALYTISCHE LÖSUNG DES EINDIMENSIONALEN ERSTARRUNGSVORGANGS IN DÜNNFLÜSSIGEN BINÄREN LEGIERUNGEN MIT GEKOPPELTER WÄRME- UND STOFFÜBERTRAGUNG

Zusammenfassung—Die Absicht dieser Studie ist es, einfache und effektive numerische und analytische Lösungsverfahren für die eindimensionale Erstarrung in dünnflüssigen binären Legierungen zu erhalten. Obwohl die numerischen und analytischen Ergebnisse hier für eindimensionale sphärische Koordinaten erstellt wurden, ist die Lösungsmethode auch für einige andere eindimensionale Erstarrungsprobleme gültig. Es wird angenommen, daß die Wärme- und Stoffübertragung nur mittels Diffusion geschieht und ein örtliches thermodynamisches Gleichgewicht an der Phasengrenze auftritt, welche eben sei. In dieser Studie werden Solidus- und Liquiduskurven als linear angenommen; es können jedoch auch allgemeine Phasendiagramme angepaßt werden. Die numerischen Ergebnisse werden für einen weiten Bereich des Diffusivitätsverhältnisses dargestellt. Das Vorhandensein steiler Konzentrationsgradienten an der Erstarrungsfront erfordert keine besondere Anpassung des numerischen Verfahrens. Mit der neuen dargestellten analytischen Methode können alle existierenden exakten analytischen Lösungen, die nur für halbunendliche Gebiete gelten, systematisch abgeleitet werden.

ЧИСЛЕННЫЕ И АНАЛИТИЧЕСКИЕ РЕШЕНИЯ ОДНОМЕРНОЙ ЗАДАЧИ ЗАМОРАЖИВАНИЯ РАЗБАВЛЕННЫХ БИНАРНЫХ СПЛАВОВ ПРИ СВЯЗАННОМ ТЕПЛО- И МАССОПЕРЕНОСЕ

Аннотация—Найдены простые и эффективные численные и аналитические решения одномерной задачи затвердевания разбавленных бинарных сплавов. Несмотря на то, что численные и аналитические результаты получены для процесса одномерного радиально симметричного внешнего сферического затвердевания, методы решения могут быть распространены и на другие одномерные задачи. Предполагается, что имеет место только диффузионный тепло- и массоперенос и на фронте замораживания существует локальное термодинамическое равновесие. Считается, что кривые солидуса и ликвидуса являются линейными, однако могут быть использованы и более общие фазовые диаграммы. Приводятся численные результаты для широких диапазонов значений отношений коэффициентов диффузии. Большой градиент концентраций на фронте плавления не требует специальных модификаций численной схемы. Предложенным аналитическим методом могут быть получены все ранее найденные аналитические решения для полуограниченной области.